23. Magnetic Resonance Imaging

Wolfgang R. Nitz

Magnetic resonance imaging (MRI) represents an exciting technology not only from a technological perspective but also in view of it's clinical potential. A brief introduction will be given with respect to the historical development of *nuclear magnetic resonance* (NMR) later to be called MRI. A MRI system can be considered primarily composed of a magnet, a magnetic field gradient system, *radio frequency* (RF) coils for signal processing. The introduction of those hardware components is followed by a description of basic MRI principles and applications. Although MRI is a noninvasive technology working without ionizing radiation, it has nevertheless a few safety aspects to be considered. The chapter will close with a speculative outlook to the future of MRI and combined modalities.

23.1 History of MRI

Wolfgang Pauli proposed the existence of a nuclear spin in 1924 [23.1]. His statement followed a year after the introduction of the spin of the electron by George Eugene Uhlenbeck and Samuel A. Goudsmit. In 1933, *Otto Stern* and *Walther Gerlach* were successful in demonstrating the existence of a nuclear spin in deviating a beam of hydrogen molecules in a magnetic field [23.2–5]. Supported by the experience of Gorter, *Rabi* of Columbia University in New York was successful in measuring the *nuclear magnetic moment* [23.6] in 1937. Earlier, Gorter had performed similar experiments, but with negative result. *Gorter* was the first to use the term *nuclear magnetic resonance* (NMR) in his publications [23.7].

It is general perception that the experiments launching the development of NMR were performed by *Bloch* and *Purcell* in 1946, proving the existence of the nuclear spin and the phenomenon of (nuclear) magnetic resonance [(N)MR] [23.8, 9], work for which Bloch and Purcell shared the Nobel Prize in 1952.

The spin is characterized by an angular momentum combined with a magnetic moment. The spin is a quantum-mechanical entity. As a consequence, the magnetic moment of the proton (with spin quantum number 1/2), exposed to an external magnetic field B_0, can only have two possible positions: parallel or antiparallel to the direction of the field. Those positions are characterized by a difference in energy, with the parallel position being energetically preferred.

If the energy of an electromagnetic wave corresponds exactly to the energy difference between these two possible states, parallel aligned spins can be pushed into the antiparallel position. With the return of the antiparallel spins back to the original parallel position, the energy difference is released as an electromagnetic wave, also called the NMR signal. As the wavelength λ of the stimulating electromagnetic field has to be identical to the wavelength representing the difference between the two possible states

$$\Delta E = \gamma \hbar B_0 = h\nu = h\frac{c}{\lambda} ,$$

which is typical for a *resonance* condition, the phenomenon is also called *magnetic resonance*.

As more spins are aligned parallel to the external magnetic field, as compared with the antiparallel alignment, a longitudinal nuclear magnetization builds up. The longitudinal nuclear magnetization can be treated using the principles of classical physics. If the longitudinal nuclear magnetization is tilted away from the parallel direction of the external magnetic field, the angular momentum of the spins causes precession of the magnetization around the original alignment (the direction of the external magnetic field B_0). This precessional frequency is called the Larmor frequency and is identical to the frequency representing the energy difference between the two quantum-mechanical states. The projection of the precessing nuclear magnetization onto the transverse plane is called the transverse nuclear magnetization. If all the longitudinal nuclear magnetization is converted to transverse nuclear magnetization, the initiating radiofrequency (RF) pulse is called a 90° RF excitation pulse. Following excitation, the longitudinal nuclear magnetization within the tissue will recover within a tissue-specific timeframe. *Bloch* introduced the term T_1 within his phenomenological Bloch equations [23.10] to characterize this *recovery time*. The mechanism of recovery is called *relaxation*, and the correlated time constant is termed the T_1 relaxation time. The precessing transverse nuclear magnetization will induce a voltage in any antenna system or coil in close vicinity to the object. The signal will decay within a tissue-specific time, which Bloch termed T_2. The underlying mechanism is called T_2 relaxation, and the time constant the T_2 relaxation time. Experiments to measure tissue-specific relaxation times on living cells and animal tissues were performed as early as 1955 [23.11]. *Damadian* at the Downstate Medical Center in Brooklyn and *Hollis* at Johns Hopkins University in Baltimore evaluated the T_1 and T_2 relaxation times of normal and cancer tissue and observed that cancerous tissue demonstrated longer relaxation times as compared with normal tissue [23.12, 13]. It was *Damadian*'s belief that he had found the ultimate technology for diagnosing cancer [23.14]. Unfortunately, he gave no practical hint regarding how to perform cancer screening on a human body.

It was the American chemist *Lauterbur* at the State University of New York who, in 1971, introduced the concept of using a magnetic field gradient superimposed on a static magnetic field to spatially encode the signal induced by the precessing nuclear magnetization [23.15]. The previously mentioned resonance frequency is a function of the strength of the magnetic field. If a magnetic field gradient is superimposed on the static magnetic field, the magnetic field strength becomes a function of location, and with this also the resonance frequency becomes a function of location. Fourier transformation (FT) can be applied to analyze the signal induced by the transverse nuclear magnetization in order to identify the frequency components indicating the location, and thereby assign a brightness to the pixel on the display representing that location, proportional to the detected amplitude.

Lauterbur used two test-tubes filled with water to demonstrate spatially encoded nuclear magnetic resonance (NMR) by superimposing a magnetic field gradient on a static magnetic field, producing a signal providing a projection of the objects. Repeating the experiment with rotated magnetic field gradients and applying the reconstruction algorithm recently established for x-ray computer tomography, he was able to produce an image of the water within the test-tubes.

In April 1974, Lauterbur gave a presentation at a scientific meeting in Raleigh, North Carolina, which was

also attended by Richard Ernst from the University of Zurich. Ernst recognized that the back-projection could be replaced by a combination of phase and frequency encoding of the MR signal [23.16]. This method is still the main reconstruction algorithm used in NMR. To avoid the fear associated with the word *nuclear*, NMR was more and more called magnetic resonance imaging (MRI) around 1981.

The British company EMI, which revolutionized medical imaging in 1973 with the introduction of the first x-ray computer tomography system, announced in 1976 the development of a scanner based on radio waves, and in 1978 presented the first image of a human head using MRI. This announcement gave a significant boost to the medical imaging industry, as they were not to repeat their mistake of underestimating the potential of a new imaging modality as they did with x-ray computer tomography. In the early 1980s, the first MR installations based on commercial products and aiming for routine clinical applications were seen.

23.2 MRI – System Components

23.2.1 The Magnet – The Magnetic Field Strength B_0

The phenomenon of magnetic resonance is only observed in the presence of a strong magnetic field. The strength of the static magnetic field B_0 is described in units of Tesla (T), at least within the medical community [for physicists, T means the magnetic flux density in units of $\mathrm{V\,s/m^2}$ and the magnetic field strength is measured in units of A/m or oerstedt (Oe)].

Early systems (1983) used resistive magnets with magnetic field strength in the range 0.1–0.2 T.

Within the same year it became obvious that superconductivity could be used to generate higher magnetic fields. Since then, the field strength used in clinical scanners has steadily increased. In 1985, the field strength of the majority of the systems was 0.5 T. Currently, in 2010, there is a strong tendency towards 3.0 T systems, whereas 1.5 T systems have the largest market share.

The primary reason for using a higher magnetic field strength is obvious: the ratio between signal and background noise (the signal-to-noise ratio, SNR) is, to a first approximation, proportional to the magnetic field strength [23.17].

The electromagnetic noise N, with its primary origin within the patient, is approximately linear in the magnetic field strength B_0

$$N \sim B_0 \,.$$

The induced MRI signal is a function of the rotating (transverse) nuclear magnetization, meaning proportional to the resonance frequency and the amplitude

$$S \sim \frac{\mathrm{d}M_{xy}}{\mathrm{d}t} \sim \nu M_{xy} \,,$$
$$\nu \sim \gamma B_0 \,.$$

The transverse nuclear magnetization M_{xy} is generated by tilting the longitudinal nuclear magnetization M_z away from the direction of the main magnetic field. If a 90° RF excitation pulse is used, all of the available longitudinal nuclear magnetization M_z is converted to transverse nuclear magnetization M_{xy}.

The amplitude of the longitudinal nuclear magnetization is a function of the occupation probability of the different energy levels (of parallel and antiparallel alignment of the nuclear spins and their correlated magnetic moments). The amplitude of the longitudinal nuclear magnetization M_z scales with the magnetic field strength used

$$M_z \sim B_0 \,.$$

Considering amplitude and frequency, the induced signal is proportional to the square of the magnetic field strength used

$$S \sim B_0^2 \,,$$

and the signal-to-noise ratio (SNR) is approximately linear in the magnetic field strength

$$\mathrm{SNR} = \frac{S}{N} \sim B_0 f\,(T_1, T_2)$$

and is of course a function of the tissue-specific relaxation times T_1 and T_2.

The increase of the SNR is only one aspect of *high-field* systems. There are a number of phenomena representing advantages and disadvantages correlated with utilization of higher magnetic field strength. T_1 relaxation times are prolonged with higher magnetic fields, and differences between tissues are often reduced, leading to a reduction of contrast in T_1-weighted images. The sensitivity to gradients in magnetic susceptibility is increased with field strength, as magnet field inhomogeneities increase proportionally to the product

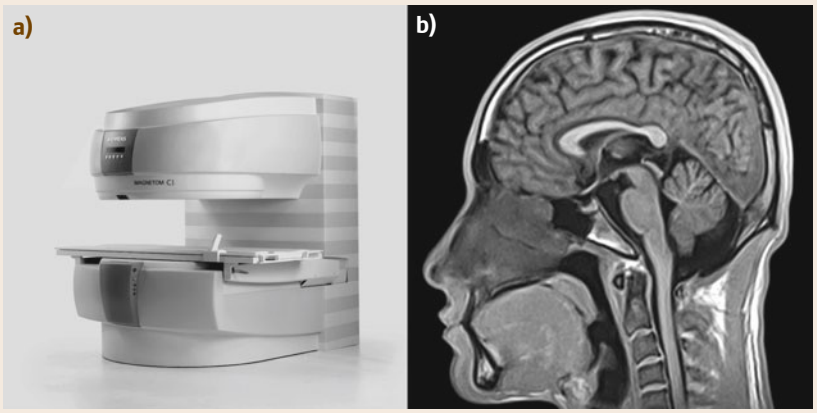

Fig. 23.1a,b A commercially available MR system using a permanent magnet with a magnetic field strength of 0.35 T (MAGNETOM C!). The T_1-weighted sagittal image of a human brain demonstrates a slice thickness of 4 mm, acquired within 5 min (courtesy Airforce General Hospital, Beijing, PR China)

of magnetic field strength and magnetic susceptibility. With the improvement in SNR, motion artifacts are no longer masked by noise and are often pronounced due to the strong signal from fat-containing moving tissue. Safety-relevant aspects need special consideration [23.18] as some potentially hazardous interactions scale with the field strength. Last but not least, the costs for an MR system scale with field strength.

Around 1991 the major vendors decided to introduce low-cost *low-field* MR systems (field strength up to 0.4 T) parallel to the *high-field* systems, as 1.0 and 1.5 T systems were called at that time. This diversity has since been maintained, and *low-field* systems are still commercially available (Fig. 23.1). A magnetic field strength of up to 0.35 T can be achieved by assembling a number of permanent magnets. Only one vendor is known to be still working with resistive magnets (stand-up MRI, FONAR Corp.). All other vendors (Siemens, General Electric, Philips, Toshiba etc.) are working with either permanent magnets or superconductive magnets. Production and maintenance of permanent systems are relatively cost effective. A disadvantage is the limitation to low field strength and the corresponding limit in SNR. Another disadvantage is the change in magnetic field strength as a function of temperature of the magnet material. Approximately 14 t of permanent magnet material is needed to achieve a field strength of 0.35 T. Resistive magnets have relatively low production costs, but are expensive in operation, have in general an extreme weight (40 t), and share the disadvantage of a temperature-dependent field strength with the permanent magnets. The production costs of superconductive magnets are relatively high, and, if helium is to be refilled regularly, they are expensive in operation, but they have the advantages of a magnetic field strength that does not change with temperature and that the generation of any reasonable magnetic field strength seems to be possible without limit and that the weight of the magnets is moderate (about 4 t for a 1.5 T system). The advantages and disadvantages of working with higher magnetic field strength will be further discussed in conjunction with safety-relevant aspects. Besides the magnetic field strength, the magnet design plays an important role that should not be underestimated. The size of the patient bore has been limited to 60 cm in the past, mainly for financial reasons, although since 2004 systems with larger patient bore openings have been available (e.g., 70 cm; Fig. 23.2). The larger opening of the patient bore is not only a comfort factor for the patient; it is also helpful in reducing the number of medical examinations refused due to claustrophobia and provides a possibility to study patients whose circumference would need more than a 60 cm bore.

23.2.2 The System for the Magnetic Field Gradient

To excite a specific slice or volume at a specific location, the MR resonance frequency, also called the Larmor frequency, has to be a function of location. For this reason, a magnetic field gradient is established in the direction of slice selection and for the duration of excitation. The slice is selected using a RF pulse whose frequency range covers the Larmor frequencies within the region to be excited. To cover all three dimensions, the magnetic field gradient coil (gradient coil) is a composition of three gradient coils arranged orthogonally to one other (x, y, z; Fig. 23.3). Sending appropriate electric currents through these coils will generate magnetic field

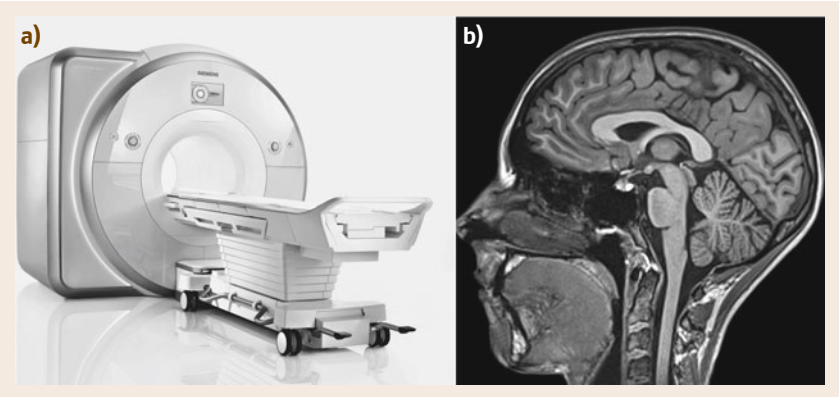

Fig. 23.2a,b Commercially available MR system using a superconductive magnet with a magnetic field strength of 3.0 T and patient bore of 70 cm (MAGNETOM SKYRA). The T_1-weighted sagittal image of a human brain demonstrates a slice thickness of 1.2 mm, acquired within 9 min

gradients that are linearly superimposed, providing the possibility of producing any arbitrary excitation plane without having to move any mechanical parts. A magnetic field gradient is also activated during the time of data acquisition. This encodes spatial information into the signal via frequency encoding, as the Larmor frequency of the emitted MR signal will be a function of location, depending on the established linear change in magnetic field strength in the direction of frequency encoding.

The electric currents I within the gradient coils will result in a Lorentz forces $\boldsymbol{F}$ in the presence of a strong magnetic field B_0

$$\boldsymbol{F} \approx \boldsymbol{I} \times \boldsymbol{B}_0 \, .$$

These forces cause vibration of the gradient coil and are the primary source of noise during an MR examination.

The amplitude of the magnetic field gradient is important with respect to achieving a good spatial resolution. A strong magnetic field gradient is also essential for diffusion weighted imaging (DWI). Wherever the amplitude time integral is of relevance, the stronger the magnetic field gradient, the shorter the encoding action. The speed of a gradient system (coil plus amplifier) is characterized by the time needed to achieve a specified gradient amplitude (ramp time). The speed primarily determines the time needed between excitation and data acquisition and directly influences the resulting image quality. The ratio between the maximum gradient amplitude and the ramp time is introduced as the *slew rate*.

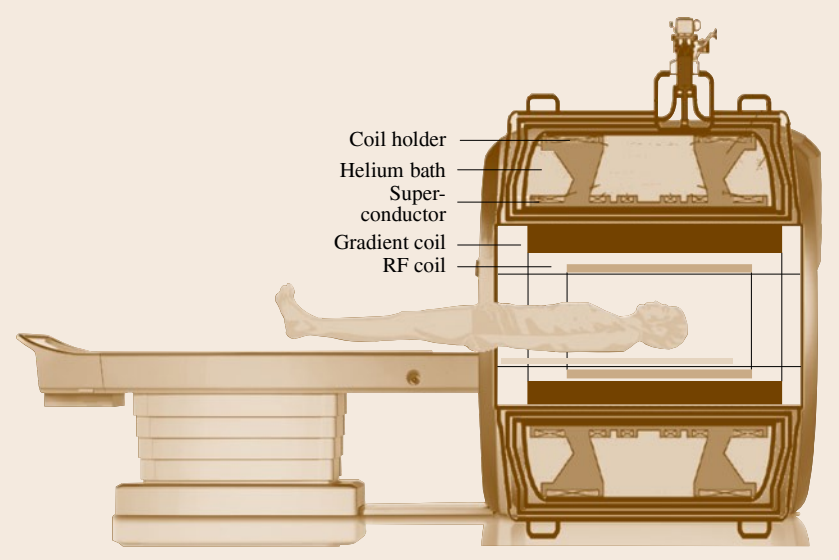

Fig. 23.3 Composition of a MR system

Air-cooled gradient coils were used in 1986 with gradient amplitudes of 3 mT/m and slew rate of 3 T/(m s). In 2003, generally available gradient amplitudes were 45 mT/m with slew rate of 200 T/(m s) using water cooling. Ramp times to establish a magnetic field gradient are between 100 and 800 μs, during which several hundred Amperes have to be maintained. To drive these currents, ≈ 2000 V are needed. The development of faster and stronger gradient systems is slightly limited by human physiology. Fast and rapid switching of magnetic field gradients induces electric potentials within the body that, with the current technology, can reach amplitudes usually used to control muscle contractions. The phenomenon is called *peripheral nerve stimulation* (PNS). As this can potentially be painful, it has to be avoided. All vendors providing strong and fast gradient systems have a *stimulation monitor* that changes imaging sequences prior to execution to avoid peripheral nerve stimulation.

Beginning with the development of MR imaging, methods have been developed and established with the aim of shortening measurement times by, e.g., undersampling of the data, with correction of the artifacts resulting from the consequent signal ambiguity using fancy algorithms. Similar approaches are currently under investigation that may allow use of faster gradient systems [23.19].

23.2.3 The Radiofrequency System

The radiofrequency system consists of a transmitter, transmit antenna, receive antenna, and receiver. Depending on the magnetic field strength used, the fundamental frequency will be 8 MHz (0.2 T) up to 128 MHz (3.0 T). The RF power amplifier has to have a peak power of several kilowatts. Since the early days of MR, a transmit antenna, also called the body coil, is located immediately behind the cover within the patient bore. The body coil is usually also able to receive the MR signal. On the other hand, placement of a receive antenna as close as possible to the patient's body (surface coil) has some significant advantages. As the patient's body emits electromagnetic noise even in the absence of excitation, and as the signal amplitude scales inversely with distance from its origin, use of a surface coil improves the SNR. Current systems utilize an array of surface coils with independent preamplifiers and/or their own receive channels for SNR optimization and for other reasons to be mentioned later. For some regions it is of advantage to use the surface coil not only as a receive coil but also as a transmit coil. In case of knee examination, an extremity coil is usually used for excitation and signal reception, exciting only the slice within the knee to be studied. The advantage is that, in transverse excitations, the adjacent knee is not excited, which otherwise would potentially lead to imaging artifacts. In case of imaging of the spine, large coil arrays, integrated into the patient table,

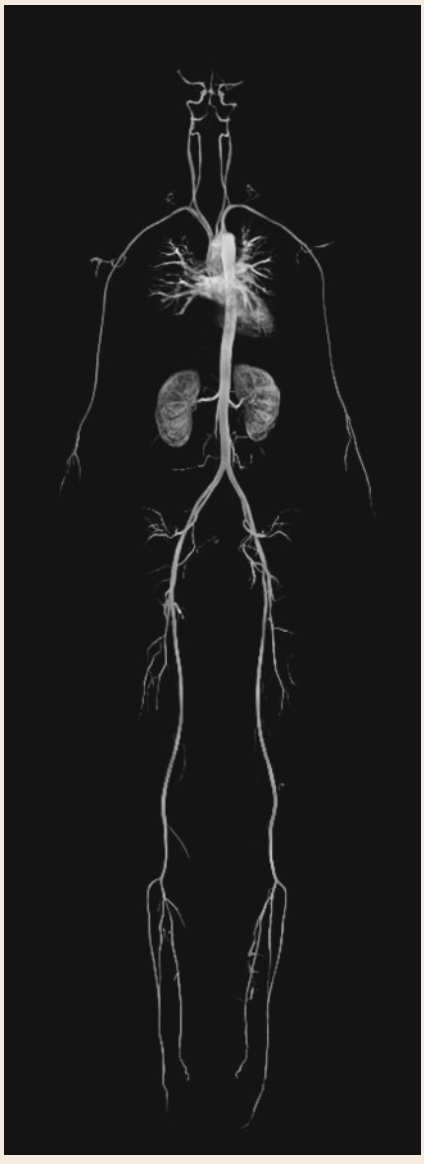

Fig. 23.4 Contrast-enhanced MR angiograph of the whole body measured within 1 min 17 s (courtesy Hong Kong Sanatorium & Hospital, Happy Valley, Hong Kong)

have been shown to be beneficial. Contrast-enhanced MR angiography studies demand an even larger surface coil coverage (Fig. 23.4) [23.20, 21]. Figure 23.5 shows a coil arrangement suitable to cover to whole vascular system from head to toe.

With the introduction of spatially distributed coil arrays, some methods evolved to utilize the spatial information provided by the coil distribution, reducing the measurement time by undersampling. As all coils receive the signal *in parallel*, the term *parallel acquisition techniques* (PAT) has been established, where the PAT factor indicates the degree of undersampling and the corresponding reduction in measurement time. The undersampling causes signal ambiguity leading to so-called *overfolding* artifacts. Prior to showing the final images to the user, a background task is to analyze the raw data or the final image of each coil to identify and remove such artifacts. The algorithm using image information for this purpose has been named *sensitivity encoding* (SENSE) [23.22]. Another algorithm applied to the signal data with the same aim of removing the above-mentioned artifacts is called *generalized autocalibrating partially parallel acquisitions* (GRAPPA) [23.23]. All these PAT techniques have one disadvantage in common: Any attempt to reduce the measurement time with the spatial resolution being held constant will result in a loss in SNR according to

$$\mathrm{SNR} \sim \frac{1}{\sqrt{\mathrm{PAT}}} \,.$$

The loss in SNR experienced when using parallel acquisition techniques can be compensated with the better SNR achievable with higher magnetic field strength. For this reason, parallel imaging techniques have shown their full potential in conjunction with high-field systems.

Besides the utilization of spatially distributed surface coils to improve the image quality or for the purpose of reducing measurement time with undersampling, it has been and still is discussed whether it would be of advantage to use spatially distributed coil arrays for transmission, so-called transmit arrays (TX arrays).

Following the term *parallel acquisition techniques* (PAT), the name *parallel transmit* (pTX) has been introduced. It seems that, with the increasing importance of high-field systems, pTX might provide some features to address some of the challenges faced when approaching higher magnetic fields. One of those challenges is the homogeneity of the excitation field, also called the B_1 field. The wavelength of the electromagnetic fields (EM) correlated with higher magnetic fields

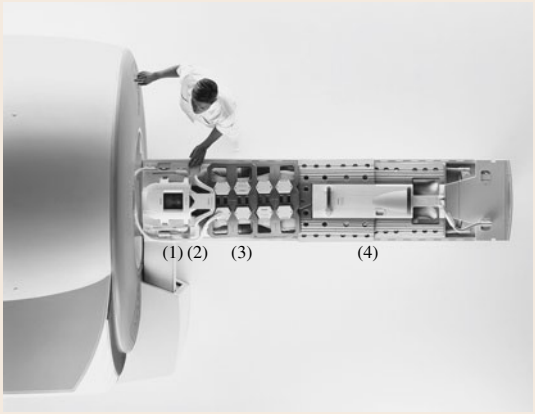

Fig. 23.5 Possible coil arrangement for a whole-body MR angiography: head coil (1), neck coil (2), body array (3), and peripheral angiography coil (4) (spine coil integrated within patient table)

B_0 is approaching the spatial dimensions of the patient's body. This leads to potential interaction of the EM field with and within the patient's body, causing B_1 inhomogeneities. The latter results in different RF excitation and/or refocusing amplitudes, leading to signal intensity changes within the image that are unrelated to anatomy. This will lead to spatial inhomogeneity of an otherwise homogeneous signal distribution within the image, unrelated to the underlying anatomy. This is of course an unwanted phenomenon. Besides other possible alternatives to compensate this artificial appearance, spatially distributed transmit coils can be used to homogenize the B_1 field.

23.2.4 Measurement Control, Acquisition, and Image Reconstruction Systems

At the beginning of the development of MR imaging, documentation of patient data, image storage, and measurement protocols were handled by a PDP-11 computer, and measurement control as well as image reconstruction were performed using vendor-specific proprietary hardware and software. In the early 1990s, most MR vendors came to the conclusion that they could benefit from the vastly evolving market of personal computers (PCs).

Most (N)MR systems today use three computer systems:

- A *host*, handling the patient data including the generated images, providing the user interface to run

the measurements, and displaying the generated images.
- A *measurement control*, providing the gradient amplifier with data necessary to establish the magnetic gradient fields on time, supplying the RF power amplifier with the necessary information, and handling the synchronization with the image reconstruction system.
- An *image reconstruction system* with the primary task of performing fast Fourier transformation. The spatial information is contained within the frequency and the phase information of the received MR signal. That information is retrieved using a Fourier transformation. Secondary tasks for the image reconstruction system are inline postprocessing algorithms that run prior to or during image reconstruction, or immediately afterwards.

In theory it is also conceivable to combine all of these tasks within one computer [23.24].

23.3 MRI – Basic Principles and Applications

MRI is a well-established modality for routine clinical imaging. In conjunction with healthcare reform, there are standards and guidelines describing as and when MRI is appropriate [23.25, 26]. To ensure the quality of diagnostic studies, these standards and guidelines are supported by matching billing codes for reimbursement [23.27]. Medicare and Medicaid service centers are constantly implementing cost-savings approaches in healthcare to ensure an affordable and adequate healthcare system [23.28]. Standards and guidelines include recommendations with respect to spatial resolution, weightings, slice orientations, and coverage. The nomenclature *weighting* is used to indicate the tissue-specific MR-related parameter that dominates the image contrast. The sources for MR signals are protons (primarily the nuclei of hydrogen atoms located within relatively freely moving water molecules). If the imaging protocol is selected such that the number of protons within a voxel dominates the signal amplitude and thereby the image contrast, the weighting is called proton density (PDw). If the factor dominating the image contrast is the speed of recovery of the longitudinal nuclear magnetization following excitation, the weighting is called T_1w. If the image contrast is dominated by the effect of the tissue-specific fading of the MR signal, the weighting is called T_2w. Based on experience acquired over decades, vendors provide programs consisting of a list of protocols for different regions (e.g., head, spin, shoulder, and knee), different weightings (e.g., PDw, T_1w, and T_2w), and different orientations (axial, transverse, coronal, tilted or any arbitrary orientation). An institution running an MR system can modify these programs based on current state-of-the-art imaging techniques, past experience, and current guidelines and recommendations, and can save these modified programs to become part of their routine clinical imaging. The basis for a measurement protocol is the essential series of actions for excitation, refocusing, spatial encoding, and data acquisition, called a *sequence*.

23.3.1 Slice Selection and Spatial Encoding

The sequence starts with ramping up of the magnetic field gradient in the direction of slice selection, as shown in Fig. 23.6. As soon as the magnetic field gradient is stable, a RF pulse is applied with a frequency range matching the Larmor frequencies within the region to be excited. A user-defined field of view and matrix define the size of a single spatial volume, called a *voxel*. The sum of all signals coming out of a single voxel defines the brightness of the corresponding pixel on the screen. The only phenomenon utilized for spatial encoding is the fact that the precessional frequency of the rotating transverse nuclear magnetization is a function of the magnetic field strength at that location. If a brief period of different rotational frequencies is utilized, the phase position of the adjacent transverse nuclear magnetizations will be altered. This is called phase encoding. Such phase encoding is usually applied directly after excitation in a direction perpendicular to the direction of slice selection. At the same point in time the expected dephasing during frequency encoding is prospectively dephased in the opposite direction to get a rephasing point during data acquisition. When switching on the frequency-encoding gradient, an *echo* is formed, and the data are acquired in the presence of a magnetic field gradient that is perpendicular to the direction of slice selection and perpendicular to the direction of phase encoding. The acquired signal is digitized according to matrix size and frequency bandwidth and is stored in a raw data matrix. As each data point

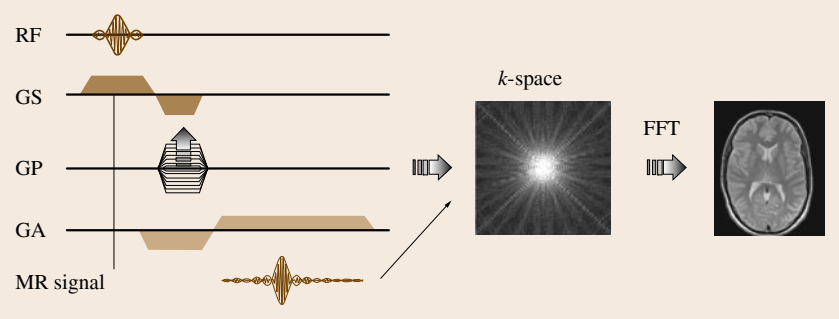

Fig. 23.6 Sequence diagram. A RF excitation pulse is applied as soon as the slice selection gradient (GS) reaches the nominal value. Following the excitation pulse, the generated but (due to the differences in resonance frequencies in the direction of slice selection during excitation) dephased transverse nuclear magnetization is rephased. During the same time period the phase-encoding gradient can be applied (GP) and the rephasing in the direction of frequency encoding can be prepared (GA) – as the transverse nuclear magnetization will dephase due to the differences in resonance frequencies as a consequence of the frequency-encoding magnetic field gradient during the readout period. Finally, the data are acquired in the presence of a frequency-encoding magnetic field gradient (GA). The data are saved into a raw data matrix, also called *k*-space. A two-dimensional fast Fourier transformation (FFT) applied to those data will lead to the final image

within the raw data matrix has an index called k, the raw data matrix is also called *k-space*. Depending on the matrix size in the direction of phase encoding, multiple repetitions with different phase-encoding gradients are required to obtain enough information to reconstruct an image.

23.3.2 The Spin-Echo Sequence

The spin echo was found accidentally during an experiment to measure a tissue-specific T_1 relaxation time [23.29]. Combined with the spatial encoding scheme of an imaging sequence it is also termed the spin-echo sequence. Initially introduced for imaging in 1983, it is still used today for T_1w imaging. Besides the already discussed tissue-specific parameters PD, T_1, and T_2, there is another imaging-relevant parameter, the magnetic susceptibility χ, which indicates whether the external magnetic field is increased (paramagnetic or ferromagnetic behavior) or decreased (diamagnetic behavior).

With this, the protons within a given tissue experience an effective magnetic field according to

$$B_{0(\mathrm{eff})} = (1+\chi)B_0 \,.$$

The Larmor frequency scales with this effective magnetic field. Biological tissue is diamagnetic in general, although differences on a scale of 10^{-6} [23.30] are considered small. For slice selection, these small differences are usually negligible. For spatial encoding, the variations of the magnetic susceptibility within the spatial dimensions of a voxel will cause different resonance frequencies, resulting in faster fading of the MR signal. This faster fading is characterized by the time constant T_2^*, given by

$$\frac{1}{T_2^*} = \frac{1}{T_2} + \gamma \Delta B \,,$$

with γ being the gyromagnetic ratio of 2.675×10^8 T^{-1} s^{-1} for the proton, and ΔB representing the magnetic field gradient caused by the difference in magnetic susceptibility. The resulting spatial distribution of different resonance frequencies is spatially fixed and constant in time. This allows the dephasing to be reversed using a so-called RF refocusing pulse. A spin-echo sequence has a 90° RF excitation pulse and also a 180° RF refocusing pulse. With this 180° RF refocusing pulse, the faster component of the transverse nuclear magnetization will be placed behind the slower component, and in the process of catching up, a spin echo is formed, which is acquired in the presence of a frequency-encoding magnetic field gradient.

Several repetitions with different phase-encoding steps are necessary to obtain enough information to reconstruct an image. The time between repetitions is called the repetition time (TR). The time between excitation and data acquisition is called the echo time (TE) (Fig. 23.7). A long repetition time (3–9 s) will suppress any influence of different T_1 relaxation times. If additionally a short echo time is selected (≤ 20 ms), dif-

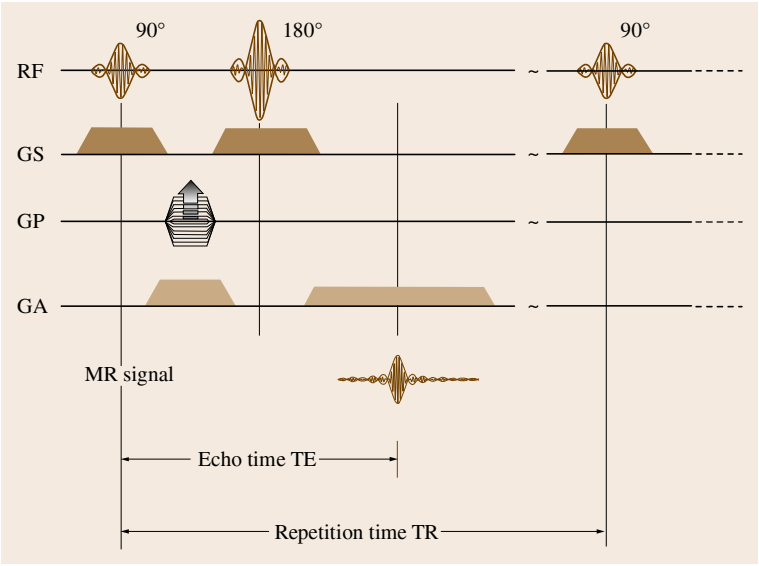

Fig. 23.7 Sequence diagram for a spin-echo sequence, illustrating the repetition time (TR) and echo time (TE)

ferences in T_2 relaxation times will be suppressed as well. Such a protocol is called proton density weighting (PDw), as primarily the number of protons per voxel will be responsible for the amplitude of the MR signal. Selecting the same repetition time but using a longer echo time will lead to a T_2-weighted (T_2w) protocol. With short echo times and relatively short repetition times (300–800 ms), T_1-weighted (T_1w) images will be acquired. The above parameters are suggested in view of the relaxation times within biological tissues (Table 23.1). The matrix size in the direction of phase encoding usually dictates the number of necessary repetitions and with this the overall measurement time. For a T_1-weighted protocol, a measurement time shorter than 5 min should be possible. As mentioned above, the excitation is a result of introducing energy into the spin system. The T_1 relaxation time is a function of how fast the spin system can release this energy to the environ-

Table 23.1 MR relaxation times for different tissues

Region		T_1 relaxation time (ms)			T_2 relaxation time (ms)
		1.5 T	1.0 T	0.2 T	
Brain	Gray matter (GM)	921	813	495	101
	White matter (WM)	787	683	390	92
	Cerebrospinal fluid (CSF)	3000	2500	1200	1500
	Edema	1090	975	627	113
	Meningioma	979	871	549	103
	Glioma	957	931	832	111
	Astrocytoma	1109	1055	864	141
Liver	Normal tissue	493	423	229	43
	Tumor tissue	905	857	692	84
Spleen	Normal tissue	782	683	400	62
Pancreas	Normal tissue	513	455	283	
	Tumor tissue	1448	1235	658	
Kidney	Normal tissue	652	589	395	58
	Tumor tissue	907	864	713	83
Muscle	Normal tissue	868	732	372	47
	Tumor tissue	1083	946	554	87

ment, the surrounding tissue. Aqueous solutions such as cerebrospinal fluid show long T_1 relaxation time and appear hypointense (dark) on T_1-weighted images. Mass lesions such as tumors often not only show displacement of normal anatomy but usually involve edema, documented by hypointense (dark) appearance on T_1-weighted images. With a few exceptions, tissues with long T_1 relaxation times usually also demonstrate long T_2 relaxation times, as a consequence of intramolecular dipole–dipole interactions within the rapidly tumbling water molecules. For this reason, pathologic tissue usually shows up as hyperintense (bright) on T_2-weighted images. The signal amplitude that later defines the brightness of the according pixel is given by

$$S \sim \frac{\mathrm{d}M_{x,y}}{\mathrm{d}t} \sim M_0 \left(1 - \mathrm{e}^{-T_\mathrm{R}/T_1}\right) \mathrm{e}^{-T_\mathrm{E}/T_2} ,$$

where M_0 represents the maximum possible longitudinal nuclear magnetization M_z that can be achieved within the given voxel. M_z is converted to transverse nuclear magnetization M_{xy} using a 90° RF excitation pulse. M_{xy} rotates with the Larmor frequency, inducing a signal in an adjacent receiver coil.

Diagnostic confidence has been increased with the introduction of T_1-shortening paramagnetic contrast agents [23.31–33]. Inflammatory lesions taking up contrast agents usually show up as very hyperintense (bright) on T_1-weighted images.

23.3.3 The Multi-Echo Spin-Echo Sequence

Images with different echo times are needed to calculate the average T_2 relaxation time within a voxel. Those images can be acquired with a single sequence containing multiple RF refocusing pulses. On viewing such images, it becomes obvious that image contrast is only slightly changing, especially for images acquired with late echoes. This observation led to the idea of acquiring another k-space line rather than producing another image. This concept will potentially significantly reduce the measurement time (Fig. 23.8).

Such a sequence has been introduced with the acronym *rapid acquisition with relaxation enhancement* (RARE) [23.34]. The image quality at the time of first introduction was rather moderate, and the method lacked attention. Seven years later, *Melki* and *Mulkern* were searching for a fast T_2-localizer and *rediscovered* the multi-echo spin-echo approach [23.35]. Likely based on progress in technology, implementation of the *localizer* revealed images with impressive quality. The surviving acronyms for the sequences that evolved out of this approach are *fast spin echo* (FSE), and *turbo spin echo* (TSE).

The advantage of this method is a significant reduction in measurement time, where the reduction is proportional to the number of echoes utilized, the so-called *echo train length* (ETL). A disadvantage should be expected due to the fact that each Fourier line has a different *weighting*. Theoretically this could lead to imaging artifacts and image misinterpretation [23.36]. In practice, the potential shortening of measurement time is not fully exploited but rather used to improve the contrast by selecting longer repetition times and increasing the spatial resolution. Both measures would prolong the measurement time, where the prolongation is now compensated by using the multi-echo approach. This leads to a significant improvement for PD- and T_2-weighted imaging and overcompensates the above-

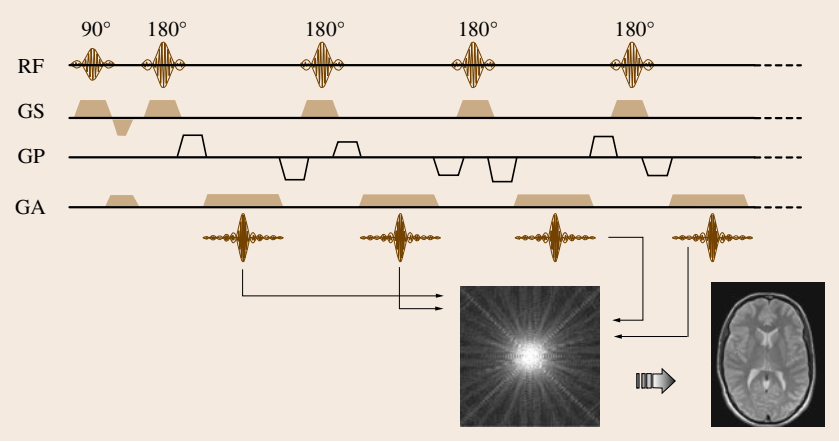

Fig. 23.8 Sequence diagram for a multi-echo spin-echo sequence [turbo spin echo (TSE), fast spin echo (FSE)]

mentioned potential disadvantages of the multi-echo approach. Today PD- and T_2-weighted imaging are solely done using FSE and TSE sequences.

23.3.4 The Gradient Echo Sequence

Omitting the 180° RF refocusing pulse leads to the generation of an *echo* by using bipolar gradient switching in conjunction with frequency encoding (Fig. 23.6). This suggested the acronym gradient-echo sequence (GRE). Different vendors use different acronyms for this generic approach, such as *fast low-angle shot* (FLASH) [23.37], *fast field echo* (FFE)-T1 or *spoiled gradient recalled acquired steady state* (SPGR). Without the use of a 180° RF refocusing pulse, the signal decay no longer follows solely the intramolecular spin–spin interaction characterized by the T_2 relaxation time, but is now also a function of local magnetic field inhomogeneities. The latter are partly introduced by the patient themselves due to differences in magnetic susceptibility of neighboring tissue. The *faster* signal decay as a consequence of all these dephasing mechanisms is characterized by the relaxation time T_2^*. It is customary in gradient-echo imaging to optimize the signal amplitude by using a low-angle excitation instead of a 90° excitation pulse. The signal response in relation to the excitation angle α in any given tissue follows

$$S \sim M_{x,y} = M_0 \frac{\left(1 - \mathrm{e}^{-T_\mathrm{R}/T_1}\right)}{1 - \cos\alpha\, \mathrm{e}^{-T_\mathrm{R}/T_1}} \mathrm{e}^{-T_\mathrm{E}/T_2^*} \sin\alpha \,.$$

GREs are used whenever short repetition times are desired. GREs are used for fast imaging and/or wherever T_2^* sensitivity is desired. As an example, GREs are applied for imaging of the beating heart (Fig. 23.9). Phase encoding is not limited to spatial encoding of the second dimension within an imaging plane, but can also be used to further *partition* a slice, in this case called a volume. This approach is called 3-D imaging. The only disadvantage is that, for every phase-encoding step in the direction of slice selection, all phase-encoding steps within the imaging plane have to be repeated. To stay within clinically practical measurement times (≤ 12 min), only gradient-echo approaches with short repetition times were suitable in the past. Gradient-echo sequences are the framework for all MR angiography methods (Fig. 23.10).

The T_2^* sensitivity is very helpful in identifying hemorrhagic lesions and is currently fully exploited

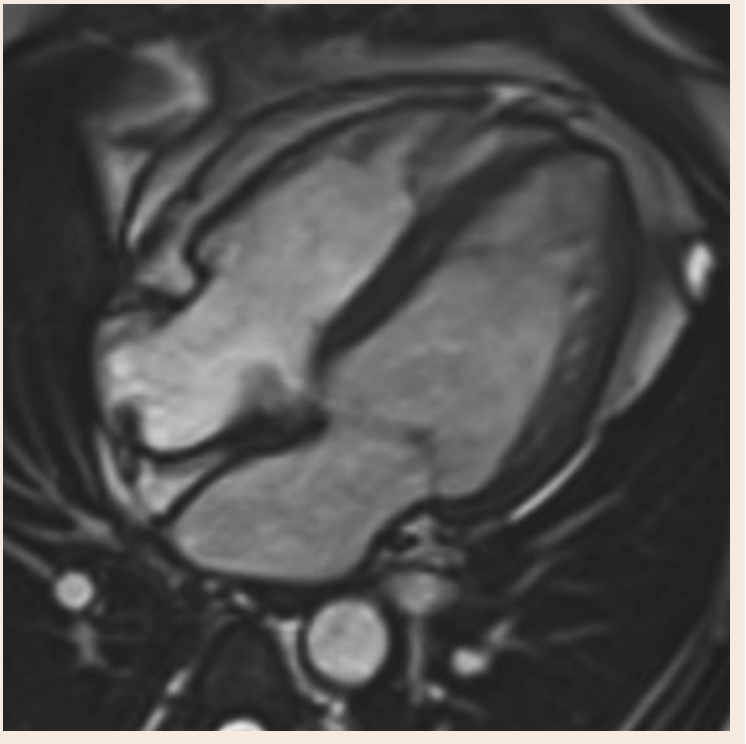

Fig. 23.9 Representation of a singe timeframe of an image of a beating heart. Measurement time was 9.28 s with temporal resolution of 43 ms (four-chamber view, myocardial infarction; courtesy of the PLA 306 Hospital, Beijing, PR China)

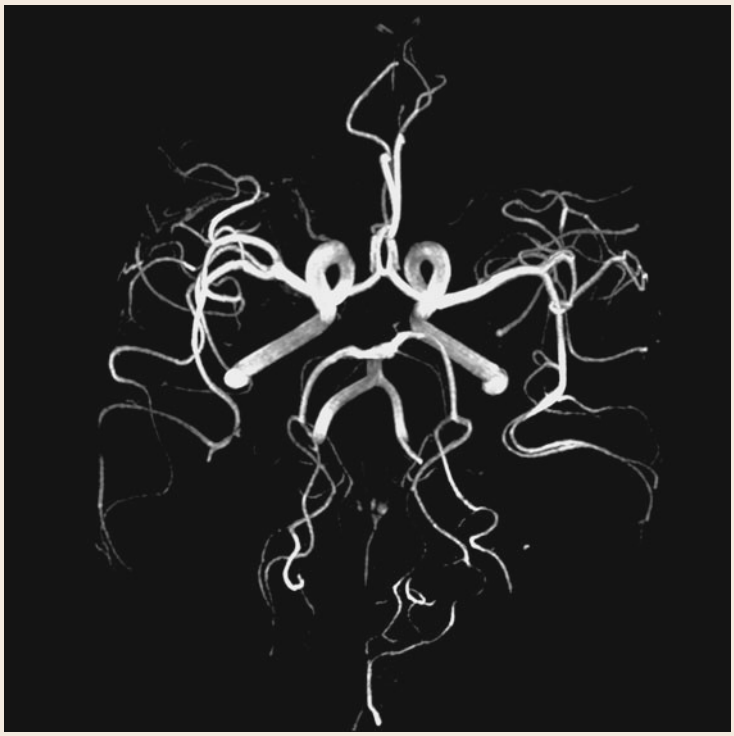

Fig. 23.10 Axial view of the intracranial vasculature generated without use of a contrast agent. The contrast is solely based on unsaturated blood flowing into the imaging volume while acquiring the data [time-of-flight MR angiography (ToF-MRA)]. Measurement time was 5.5 min

in *susceptibility-weighted imaging* (SWI) [23.38]. The change in oxygen concentration within the blood vasculature of active brain regions is correlated with alteration of the magnetic susceptibility and is used in *blood oxygenation-dependent imaging* (BOLD) to visualize active brain regions. As this allows the function of the brain to be documented, it is also called *functional MRI* (fMRI) [23.39, 40]. In conjunction with intravenous injection of paramagnetic contrast agents, the correlated changes in magnetic susceptibility as a marker for the passage of the contrast agent can be used to trace and document perfusion deficits when using T_2^*-sensitive protocols [23.41, 42]. One further feature of gradient-echo sequences is worth mentioning. This feature is important for diagnosis of benign or malignant abdominal mass lesions. Protons of hydrogen atoms within lipids have a resonance frequency that is about 3.5 ppm lower than the resonance frequency of protons contained in hydrogen atoms within freely moving water molecules. This is due to the differences in the electronic environment (oxygen versus carbon). This will cause slower rotation of the transverse nuclear magnetization within lipids as compared with water, a phenomenon called *chemical shift*. In spin-echo imaging, the 180° RF refocusing pulse places the faster component of the rotating transverse nuclear magnetization behind the slower component, and at the time the echo reaches its maximum, both transverse nuclear magnetizations are in phase again and only the image shift in the direction of spatial encoding will remain. In GRE imaging there is no RF refocusing pulse, and depending on the echo time, there will be a situation where the transverse nuclear magnetization within lipids will be in *opposed-phase* with the transverse nuclear magnetization within water, whereas at a later echo they will be *in-phase* again. In the *antiphase* case the net signal will be zero for a voxel, with fat and water showing approximately identical transverse nuclear magnetizations. The corresponding pixel will show up dark due to the signal void. As fat-containing mass lesions are usually benign, this can be used to differentiate benign adenomas from malignant metastases [23.43].

23.3.5 The Sequence Family

The subjective impression is that SE, GRE, and the multi-echo concepts of FSE or TSE are the most im-

portant imaging sequences for current routine clinical imaging. In any case, all existing imaging sequences can be characterized as belonging to either the SE or the GRE group [23.44], with different types of hybrids. Worth mentioning is the possibility of manipulating the longitudinal or transverse nuclear magnetization prior to or within an imaging sequence. A classic example is the inversion of the longitudinal nuclear magnetization prior to starting the imaging sequence. Such inversion allows the signal of a tissue with a specific T_1 relaxation time to be nulled. Tissue is only able to emit a signal if longitudinal nuclear magnetization is available at the time of excitation. The RF excitation pulse will convert the longitudinal nuclear magnetization to transverse nuclear magnetization which rotates with the Larmor frequency, inducing an MR signal in a coil adjacent to the object to be imaged. Following inversion, the inverted longitudinal nuclear magnetization will approach the parallel alignment with the main magnetic field within a time given by the T_1 relaxation time of the tissue. There is a point in time at which the longitudinal magnetization will be zero, occurring at the point of transition between antiparallel to parallel alignment. If the excitation pulse is placed at that point in time, that tissue with a specific T_1 relaxation time will not be excited. Lipids have a relatively short T_1 relaxation time. On selecting a short time period between inversion and excitation pulse, e.g., 150 ms, the signal from lipids will be suppressed. The time between inversion and excitation pulse is called the inversion time T_I. As a 150 ms inversion time was considered short at the time, the acronym short-tau inversion recovery (STIR) was established [23.45]. At the other end of the scale of relaxation times is the relative long time of freely moveable water molecules. If a long inversion time is selected (e.g., 2.5 s), the signal from fluid is suppressed, leading to the acronym *fluid-attenuated inversion recovery* (FLAIR) [23.46]. Such a protocol is helpful to identify benign cystic lesions and to identify periventricular lesions that might otherwise remain unnoticed in the presence of adjacent bright signal from cerebrospinal fluid. The recovery of longitudinal nuclear magnetization following inversion follows

$$M_z = M_0 \left(1 - 2\mathrm{e}^{-T_\mathrm{I}/T_1} + 2\mathrm{e}^{-(T_\mathrm{R}-T_\mathrm{E}/2)/T_1} - \mathrm{e}^{-T_\mathrm{R}/T_1}\right) .$$

A further important application is the preparation of the transverse nuclear magnetization in *diffusion-weighted imaging* (DWI). In the presence of diffusion, a bipolar magnetic field gradient amplitude will lead to a dephasing, resulting in a signal void [23.47]. The effect on the signal can be characterized by the so-called *b*-value

$$b = \gamma^2 G_\mathrm{DW}^2 \delta^2 \left(\Delta - \frac{\delta}{3}\right) ,$$

with G_DW being the amplitude of the diffusion-weighting magnetic field gradient, δ represents the duration of the magnetic field gradient, and Δ indicates the temporal distance between the two gradient lobes. In routine clinical imaging, *b*-values of up to 1000 s/mm^2 are customary.

The signal is as follows

$$S \sim \mathrm{e}^{-bD} ,$$

with D being the *apparent diffusion coefficient* (ADC). As the diffusion is a tensor, *diffusion tensor imaging* (DTI) will enable the measurement of the preferred diffusional direction [23.48] with an according graphical representation [23.49]. The preferred diffusional direction of water molecules seems to be parallel to nerve sheets. The diffusional directivity of these water molecules indirectly allows the display of nerve fiber tracts.

23.3.6 MRI Spectroscopy

Different nuclei have different Larmor frequencies, and identical nuclei have different Larmor frequencies depending on their electronic environment. This phenomenon is exploited in MR spectroscopy (MRS) to measure the levels of different metabolites in body tissues. The shift in Larmor frequency as a function of the electronic environment is usually described in parts per million (ppm) with respect to a reference frequency (usually free water); for example, the resonance frequencies of hydrogen nuclei in amino acids such as *N*-acetyl-aspartate (NAA) found in neurons are shifted by 2 ppm relative to the spectral line of free water. Fourier transformation following data acquisition without a readout magnetic field gradient will lead immediately to a display of spectral lines, with the amplitudes of individual lines representing the concentration of the underlying metabolites. MRI spectroscopy enables chemical analysis of tissue without biopsy, although the number of detectable chemicals is rather limited. To achieve spatial resolution in MRI spectroscopy a dual echo can be applied, for example, a 90° RF excitation pulse and two 180° RF refocusing pulses applied in the presence of magnetic field gradients that

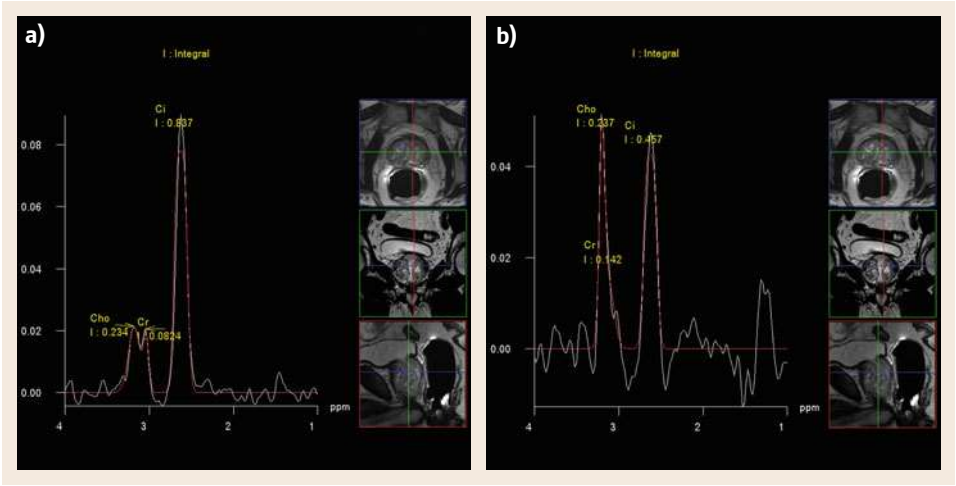

Fig. 23.11 (a) Proton MRI spectroscopy of a healthy prostate. (b) Proton MRI spectroscopy of a prostate carcinoma (courtesy of the University Hospital Mannheim)

are perpendicular to each other. The final signal will come out of the voxel represented by the intersection of the three orthogonal slices. The currently achievable voxel size is about 2–8 ml (for proton spectroscopy).

Besides proton spectroscopy, phosphorus spectroscopy should be mentioned. In this case, phosphorus is utilized as the signal-emitting nucleus.

Proton spectroscopy is mainly applied to the brain, whereas phosphorus spectroscopy is utilized to study muscles, as phosphorus allows detection of energy metabolism. In confirming the diagnosis of a prostate carcinoma, proton spectroscopy demonstrates a lowering of the citrate peak and an increase of the choline peak as compared with a normal prostate. Citrate is produced by prostate tissue. Prostate carcinomas consume citrate, and the intracellular content of citrate will be lowered. Choline is part of the cell membrane and in malignant prostate lesions, in conjunction will cell proliferation, the choline level is increased (Fig. 23.11).

23.4 MRI – Safety-Relevant Aspects

For the time period 1995–2005, the Food and Drug Administration (FDA) database shows 389 entries where humans have been harmed in conjunction with MRI. Ten percent of these accidents were related to ferromagnetic objects attracted by the strong magnetic field. Seventy percentage were related to burns caused by RF interactions. The most important safety issues can be summarized as follows:

- Attractive forces by the strong magnetic field
- Significant torques within the strong magnetic field
- RF interaction with the patient's body
- RF interaction with active or passive implants
- Peripheral nerve stimulation (PNS) caused by the rapid switching of the large magnetic field gradient amplitudes
- Acoustic noise due to the Lorentz forces on conductors with electric currents flowing in the presence of a strong magnetic field
- Cold gases in case of loss of superconductivity (quenching)
- Nephrogenic systemic fibrosis (NSF), in conjunction with Gd-containing contrast agents.

23.4.1 Attraction and Torque Due to Strong Magnetic Fields

Attractive forces on ferromagnetic objects are a consequence of a change in energy as a function of location

$$F = \nabla U \,.$$

The potential energy is the product of the magnetic moment and the applied external magnetic field

$$U = \tfrac{1}{2}\boldsymbol{M}\boldsymbol{B}_0 \,; \quad \boldsymbol{M} = \frac{\chi}{\mu_0} V \boldsymbol{B}_0 \,.$$

The magnetic moment M of a ferromagnetic object is the product of its volume V, its magnetic susceptibility χ, and the magnetic field strength at the current

location B_0. Simplified to the view of a single dimension, the attractive force on a ferromagnetic object is proportional to the magnetic field gradient at the current location and the magnetic field strength at that location

$$F_z = \frac{\chi V}{\mu_o} \boldsymbol{B}_0 \frac{\partial \boldsymbol{B}_0}{\partial z} .$$

For a pair of scissors with weight of 0.4 lb, the horizontal maximum pulling force for a 1.5 T system is approximately 20 times higher than the gravitational force, comparable to a weight of 8 lb. The critical aspect is the discontinuity of the force, which is rapidly changing as a function of location. The maximum attractive force is experienced in the vicinity of the patient bore, whereas the attractive force at the isocenter of the magnet is zero. A ferromagnetic geometrically asymmetric object will have a strong tendency to align its long axis parallel to the direction of the magnetic field. Ferromagnetic scissors will always fly into the magnet with their pointed tip entering first. The torque is proportional to the square of the magnetic field strength and is at its maximum at the isocenter of the magnet.

23.4.2 RF Interaction with the Patient's Body

The power spectrum of the electromagnetic radiation used in MRI is too weak to lead to ionization, molecular destruction, or generation of free-radical molecules. The applied energy will only lead to warming of the patient. The power W absorbed by the patient is proportional to the square of the resonance frequency of the system ω_0 (which is proportional to the magnetic field strength used) and proportional to the square of the magnetic component B_1 of the electromagnetic radiation used. The power W absorbed by the patient is proportional to the fifth power of the circumference b of the patient and inversely proportional to the internal conductivity ρ

$$W \approx \frac{\omega_0^2 B_1^2 b^5}{\rho} .$$

Acceptable levels of power deposition into a patient are documented in the international guideline on safety requirements in MR (IEC 60601-2-33). The metabolic rate of the average patient is about 90 W. This is the energy per unit time needed to maintain body temperature. IEC 60601-2-33 allows power deposition of up to 2 W/kg without medical supervision. With a body weight of 176 lb this means 160 W for the duration of the MR measurement. Doubling of the power deposition (4 W/kg) is allowed under medical supervision, and this corresponds to the metabolic rate of a marathon runner. All vendors have to ensure that their systems will refuse to start a measurement where the patient will be exposed to an energy level beyond these guidelines.

Another known potential complication is examination of patients with permanent cosmetics and tattoos. Studies have reported transient, sometimes painful skin irritation, cutaneous swelling or heating sensations, in about 1.5% of these cases. If the patient communicates painful sensations, the MR measurement can and will be aborted by the technologist running the system. There are no reports that any of this damage is of permanent nature. Swelling, reddening or blistering have so far been temporary.

23.4.3 Interaction with Active and Passive Implants

In general, all active and passive implants are of concern [23.50]. The static magnetic field strength will dislodge ferromagnetic implants, if the torque and attraction exceed the holding force. This is reported to be the case for older pacemakers, older cochlear implants, and older aneurysm clips. Orthopedic implants are in general nonferromagnetic and do not present a contraindication to MRI study. The static magnetic field is also potentially harmful to the function of active implants such as older pacemakers. The industry involved in design and production of implants is, of course, aware of the importance of MR for today's diagnostic radiology, and is anxious to introduce MR-compatible products. There are already a number of publications dealing with the MR compatibility of some pacemaker designs and neurostimulators. Especially for active implants, the concern is not limited to the static magnetic field. The coupling of the applied RF should not be underestimated. The potential coupling of the RF with, e.g., pacemaker leads, remains a risk, even if this is considered a potentially low risk.

23.4.4 Interaction Based on Changes in Magnetic Field Gradients

Peripheral Nerve Stimulation (PNS)

The law of induction indicates that a temporal change in the magnetic field strength will induce a voltage

$$\oint_{\partial S} E \, \mathrm{d}l = -\frac{\partial}{\partial t} \iint_S B \, \mathrm{d}A .$$

The human body can present conductive loops, despite its poor conduction. Depending on the orientation

of the switched magnetic field gradients, the amplitudes and switching times of today's gradient systems are capable of inducing voltages and currents within the human body that mimic biochemical voltages usually applied to control muscle contraction. Vendors are obliged to provide measures to prevent painful patient experience during MR examination. Such a measure is called a *stimulation monitor*.

Noise Exposure During MR Examination

A conductor carrying a current in the presence of a magnetic field will experience a mechanical force, known as the Lorentz force after the Dutch physicist Hendrik Antoon Lorentz who described it. The current of up to 600 A flowing through a gradient coil located within a 1.5 T system will experience a force on a single wire on the order of 2.827 kN equivalent to a weight of 635 lb. That force will remain active for the duration of the magnetic field gradient being switched on and will vanish at the time the magnetic field gradient is switched off. The duration of a slice selection gradient is about 2.5 ms. The change from force to no force is 200 Hz, which generates a tone between a musical *a* (220 Hz) and a *g* (196 Hz). For a frequency bandwidth of 195 Hz/voxel, the duration of the frequency-encoding gradient will be 5.128 ms. The switching rate of the gradient would be 97.5 Hz, which is close to a *G* (98 Hz). Unfortunately the switching of magnetic field gradients is rarely sinusoidal, and different tasks require different switching frequencies, so the final noise is rarely considered harmonic. It is required that the noise level for a patient remain below 99 dB(A) with or without ear-protective devices. No vendor is allowed to introduce a scanner to the market capable of generating more than 140 dB(A).

23.4.5 Safety Issues in Conjunction with Loss of Superconductivity (Quenching)

The loss of superconductivity of the current-carrying coil of the main magnet is called a *quench*. Currently commercially available and relatively easy to handle superconducting wires are composed of niobium, NiTi, or Nb_3Sn and are placed in about 1800 l of liquid helium at a temperature of −269 °C in order to be and remain superconductive. Loss of superconductivity is rarely sporadic (usually occurring during ramping up of the main magnetic field) but may be provoked by pressing the emergency button (the quench button). As the superconductive magnet becomes resistive, the energy stored in the now decaying magnetic field will be transferred to the liquid-helium bath, resulting in vaporization of helium. After five seconds the pressure build-up in the cryostat will be high enough to activate the blowout disc, as planned in such circumstances. The evaporating coolant is directed out of the building through a *quench pipe*. Within 1 min the coil currents have reached a zero value and the magnetic field is zero. After 2 min, the vaporization of the helium is down to a negligible level. The temperature of the evaporating helium is close to −269 °C, and the surrounding environment will be cooled accordingly. There remains the danger of burns when touching covers that were affected by the evaporating helium. In case of a blockage of the quench pipes, the helium gas will be forced into the scanner room and there will be the danger of displacement of oxygen. In that case, the scanner room is to be evacuated. Measures are to be planned and exercised to prepare for such an emergency. There are no known cases where humans have been harmed in case of a quench.

23.4.6 Gadolinium-Containing Contrast Agents and NSF

In contrast to iodine-containing contrast media, gadolinium-containing MR contrast agents were long considered non-nephrotoxic with very low risk of adverse reactions or other complications. The enthusiasm even triggered suggestions to use gadolinium-containing contrast agents in conjunction with x-ray imaging [23.51, 52]. In 2006, a group of scientists at AKH in Vienna published a study of nine end-stage renal disease patients who underwent MR angiography using a gadolinium chelate (gadolinium-diethylenetriaminepentaacetic acid bis-methylamide (Gd-DTPA-BMA)) over a period of approximately 2 years, of whom five patients developed nephrogenic fibrosing dermopathy (NFD), also called nephrogenic systemic fibrosis (NSF) [23.53, 54]. Nephrogenic systemic fibrosis involves fibrosis of skin, joints, eyes, and internal organs. The disease was first published in 2000 and has a mortality rate of 5%. Since 2006 it has been suspected and later confirmed that the disease is associated with exposure to gadolinium. Currently there are approximately 500 reported cases that can be linked to administration of Gd-containing contrast agents. Considering the approximate number of 21.5 million MR studies with MR contrast agents per year, the number of cases seems to be rather low. Nevertheless, the reported risk of Gd-containing contrast agents has to be acknowledged.

23.5 MRI – Pictures of the Future

For the past 20 years it has frequently been predicted that developments within the area of magnetic resonance and magnetic resonance imaging would reach maturity, and further progress would be slow and only incremental – similar to the development in x-ray computed tomography. So far we are still waiting for those times.

23.5.1 Magnetic Field Strength

About two-thirds of the market is currently working with magnetic field strength of 1.5 T. High-field systems with magnetic field strength of 3.0 T have a market share of about 20%, and the remaining devices are low-field (≤ 0.5 T) MR systems. Magnets with even higher magnetic field strength (7 T) are still limited to academic institutions, but there are already 37 installations known. It should also be mentioned that there are at least two 9.4 T installations and two 11.7 T systems, and of course this refers to magnets with a bore diameter suitable to study humans.

23.5.2 RF Technology

The signal gain when working with higher magnetic field strength (Fig. 23.12) is supplemental and supports measures to reduce measurement times in conjunction with the utilization of spatial information from distributed coil matrices. Otherwise, measurement of spatial information would involve time-consuming additional phase-encoding steps. The ability to use coil matrices for *parallel imaging* is a function of the number of coils and coil profiles. Modern commercial MR systems are currently prepared to serve coils of up to 128 independent receiver channels, and the first prototype coils are available. Direct digitization within the transmitter chain as well as the receiver chain has just been introduced into commercial systems and will enable future application developments.

23.5.3 Application Development

For development of new MR applications the following fields deserve special attention:

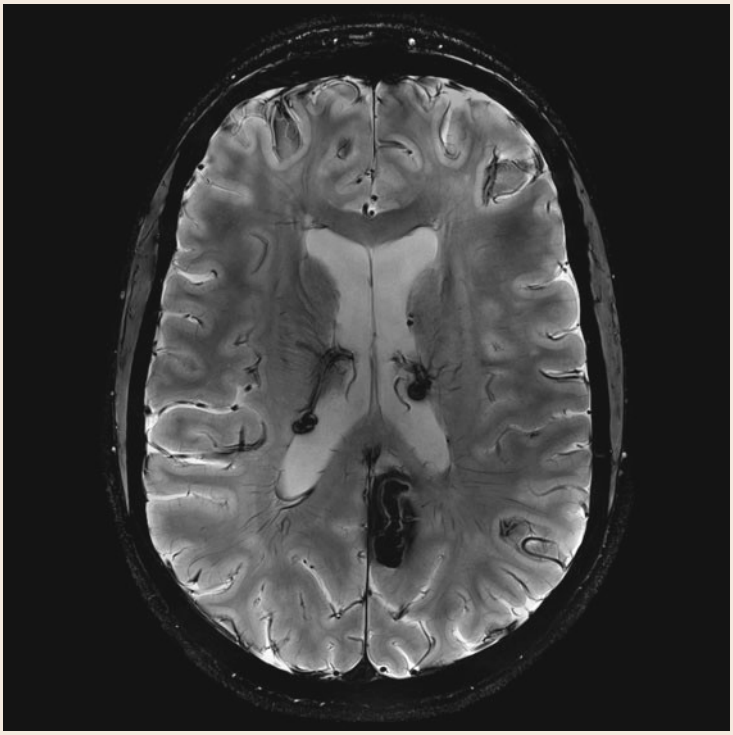

Fig. 23.12 Image of a T_2-weighted axial cut of the brain of a patient with multiple sclerosis, performed on a 7.0 T system (courtesy of the University Hospitals of New York)

- Motion correction, registration, and mapping of anatomic structures
- Mapping and visualization of different (additional) information (parametric imaging)
- Perfusion measurements without contrast agents (arterial spin labeling (ASL))
- MR angiography without contrast agents (native)
- Time-resolved contrast-enhanced MR angiography (time-resolved imaging with interleaved stochastic trajectories (TWIST) and time-resolved imaging of contrast kinetics (TRICKS))
- MR data acquisition in the presence of a continuously moving patient table (TimCT – total imaging matrix with continuous table movement, MDS – move during scan).

In general it can be stated that the current standardization and automatization is streamlining the workflow, resulting in shorter times during which patient has to remain in the scanner, while simultaneously ensuring reproducible results; e.g., for brain studies, slice orientations and coverage are recommended in specific guidelines. In modern current systems a three-dimensional localizer is usually initiated automatically after the patient has been positioned. Current modern systems are immediately able to adjust the next imaging protocol with respect to angulation and requested coverage in automatically analyzing the 3-D-localizer for anatomical structures and landmarks. Similar approaches are currently already available to automatically position required slices and volumes for studying the knee of a patient. For imaging the heart, current modern systems utilize the localizer to select the recommended short-axis or long-axis views automatically. In imaging the spine, a single mouse click can indicate to the system which intervertebral disc space is to be evaluated, and the system will automatically adjust the imaging plane to have the same angulation as the disc.

The number of selected elements of a surface coil will affect the coverage as well as the image noise. If more coil elements are selected than needed, the image noise is unnecessarily increased. If the number of coil elements selected is too low, the coverage necessary for a diagnosis may be insufficient. Current modern systems automatically select or deselect required or unnecessary coil elements.

23.5.4 Hybrid Systems

Following the success of positron emission tomography–computed tomography (PET-CT), the idea of a MR-PET system as a hybrid technology has also surfaced within the MR community. The introduction of an MR-PET system as a routine clinical modality is only a question of time. MR-PET combines complementary modalities. The superior ability of MR to display soft tissue contrast is combined with the unique feature of PET to provide biochemical information.

Potential scientific applications are:

- Simultaneous activation studies by PET and fMRI (real-time information correlation)
- PET combination with diffusion tensor imaging (DTI), three dimensional chemical shift imaging (3-D-CSI), and high-resolution structural MRI
- Dynamics of distribution of pharmaceutical products within anatomical structures
- Development and evaluation of cell therapy (stem-cell migration tracking and differentiation).

Potential clinical applications are:

- Differential diagnosis of recurrent tumors versus radiation necrosis
- Early diagnosis of Alzheimer's disease – improved prognosis due to potentially earlier medication
- Staging, restaging, and therapy monitoring in pediatric oncology
- Whole-body tumor staging and therapy monitoring
- Myocardial infarction: differentiation between hibernation and stunning.

There are a few challenges to be mastered in integrating a PET system within a MR system, starting with the development of a MR-compatible PET detector

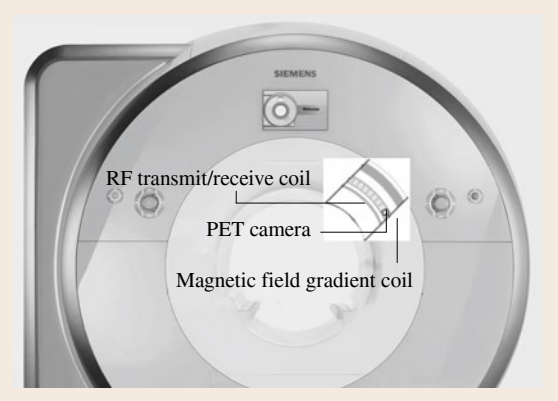

Fig. 23.13 Schematic sketch of a fully integrated MR-PET system

(Fig. 23.13). Beneficial for this development has been the early introduction of MR systems with a larger bore diameter.

23.5.5 Theranostics – Therapy Under Image Guidance

Another future possibility is the combination of an imaging modality such as MR with a therapy system such as radiation therapy. Patient position and immobilization in radiation therapy has been and still is a challenge. As of today there are no established solutions to treat cancer close to organs that permanently move due to breathing. The inherent and inevitable internal organ motion causes the tumor to be in different positions when treatment occurs, and it is impossible to determine where the dose is actually going. In the near future, continuous imaging – with MRI – will allow guidance of the focus of radiation therapy to ensure effective treatment.

As is obvious from the above, physicists and engineers as well as physicians and technologists will face an extremely exciting and interesting future in view of all these potential new and novel developments.

Further Reading

- P. Reimer, P.M. Parizel, F. Stichnoth: Clinical MR Imaging: A Practical Approach, (Springer, Berlin Heidelberg 2010)
- M.F. Reiser, W. Semmler, H. Hricak: Magnetic Resonance Tomography, (Springer, Berlin Heidelberg, 2008)
- A. Oppelt (Ed.): Imaging Systems for Medical Diagnostics, (Publicis Corporate, Erlangen 2005)
- V.M. Runge, W.R. Nitz, S.H. Schmeets: The Physics of Clinical MR Taught Through Images, (Thieme, New York Stuttgart 2009)
- C. Westbrook, C. Roth, J. Talbot: MRI in Practice, (Blackwell, Oxford 2005)

References

23.1 W. Pauli: Zur Frage der theoretischen Deutung der Satelliten einiger Spektrallinien und ihrer Beeinflussung durch magnetische Felder, Naturwissenschaften **12**(37), 741–743 (1924)

23.2 I. Estermann, O. Stern: Über die magnetische Ablenkung von Wasserstoff-Molekülen und das magnetische Moment des Protons, Z. Phys. **85**, 17 (1933)

23.3 R. Frisch, O. Stern: Über das magnetische Moment eines rotierenden Wasserstoffmoleküls, Z. Phys. **85**, 4 (1933)

23.4 W. Gerlach, O. Stern: Über die Richtungsquantelung im Magnetfeld, Ann. Phys. **74**, 673–699 (1924)

23.5 W. Gerlach, O. Stern: Das magnetische Moment des Silberatoms, Z. Phys. **9**(1), 353–355 (1922)

23.6 I.I. Rabi, J.R. Zacharias, S. Millman, P. Kusch: A new method of measuring nuclear magnetic moment, Phys. Rev. **53**, 318 (1938)

23.7 C.J. Gorter, L.J.F. Broer: Negative result of an attempt to observe nuclear magnetic resonance in solids, Physica (The Hague) **9**, 591 (1942)

23.8 F. Bloch, W.W. Hanson, M. Packard: Nuclear induction, Phys. Rev. **69**, 127 (1946)

23.9 E.M. Purcell, H.C. Torrey, R.V. Pound: Resonance absorption by nuclear magnetic moments in a solid, Phys. Rev. **69**, 37–38 (1946)

23.10 F. Bloch: Nuclear induction, Phys. Rev. **70**, 460–473 (1946)

23.11 E. Odeblad, B.N. Bhar, G. Lindström: Proton magnetic resonance of human red blood cells in heavy water exchange experiments, Arch. Biochem. Biophys. **63**, 221–225 (1956)

23.12 R.V. Damadian: Tumor detection by nuclear magnetic resonance, Science **171**, 1151–1153 (1971)

23.13 D.P. Hollis, J.S. Economou, L.C. Parks, J.C. Eggleston, L.A. Saryan, J.L. Czeisler: Nuclear magnetic resonance studies of several experimental and human malignant tumors, Cancer Res. **33**, 2156–2160 (1973)

23.14 R. Damadian: Apparatus and method for detecting cancer in tissue awarded, US Patent 3789832 (1974)

23.15 P.C. Lauterbur: Image formation by induced local interactions: Examples of employing nuclear magnetic resonance, Nature **242**, 190–191 (1973)

23.16 A. Kumar, D. Welti, R.R. Ernst: NMR Fourier zeugmatography, J. Magn. Res. **18**, 69–83 (1975)

23.17 W.A. Edelstein, G.H. Glover, C.J. Hardy, R.W. Redington: The intrinsic signal-to-noise ratio in NMR imaging, Magn. Reson. Med. **3**(4), 604–618 (1986)

23.18 C.K. Kuhl, F. Träber, H.H. Schild: Whole-body high-field-strength (3.0-T) MR imaging in clinical practice. Part I. Technical considerations and clinical applications, Radiology **246**(3), 675–696 (2008)

23.19 J. Hennig, A.M. Welz, G. Schultz, J. Korvink, Z. Liu, O. Speck, M. Zaitsev: Parallel imaging in non-bijective, curvilinear magnetic field gradients: A concept studym, MAGMA **21**(1–2), 5–14 (2008)

23.20 M.R. Prince, E.K. Yucel, J.A. Kaufman, D.C. Harrison, S.C. Geller: Dynamic gadolinium-enhanced three-

dimensional abdominal MR arteriography, J. Magn. Reson. Imaging **3**(6), 877–881 (1993)
23.21 M.R. Prince, D.L. Narasimham, J.C. Stanley, T.L. Chenevert, D.M. Williams, M.V. Marx, K.J. Cho: Breath-hold gadolinium-enhanced MR angiography of the abdominal aorta and its major branches, Radiology **197**(3), 785–792 (1995)
23.22 K.P. Pruessmann, M. Weiger, M.B. Scheidegger, P. Boesiger: SENSE: Sensitivity encoding for fast MRI, Magn. Reson. Med. **42**(5), 952–962 (1999)
23.23 M.A. Griswold, P.M. Jakob, R.M. Heidemann, M. Nittka, V. Jellus, J. Wang, B. Kiefer, A. Haase: Generalized autocalibrating partially parallel acquisitions (GRAPPA), Magn. Reson. Med. **47**(6), 1202–1210 (2002)
23.24 G. Vassalo, M. Boltano, J. Linardos, J. Damadian, J.J. Cohen, R.V. Damadian: Control of MRI System, US Patent 6157194 (2000)
23.25 American College of Radiology: ACR Appropriateness Criteria, http://www.acr.org/ (last accessed June 2, 2011)
23.26 American College of Radiology: ACR Guidelines and Standards, http://www.acr.org/ (last accessed June 2, 2011)
23.27 Durable Medical Equipment (DME): Billing Codes and Reimbursement Rates, http://www.findacode.com/hcpcs (last accessed June 2, 2011)
23.28 Centers for Medicare and Medicaid Services (CMS): Healthcare Common Procedure Coding System (HCPCS), http://www.cms.gov/MedHCPCSGenInfo (last accessed June 2, 2011)
23.29 E. Hahn: How I stumbled across the Spin Echo, Third Annual Lauterbur Lecture, Proceedings of the International Society of Magnetic Resonance in Medicine (Philadelphia 1999)
23.30 P.W. Kuchel, B.E. Chapman, W.A. Bubb, P.E. Hansen, C.J. Durrant, M.P. Hertzberg: Magnetic susceptibility: Solutions, emulsions, and cells, Concepts Magn. Reson. **18A**, 56–71 (2003)
23.31 V.M. Runge, J.A. Clanton, W.A. Herzer, S.J. Gibbs, A.C. Price, C.L. Partain, A.E. James Jr.: Intravascular contrast agents suitable for magnetic resonance imaging, Radiology **153**(1), 171–176 (1984)
23.32 H.P. Niendorf, R. Felix, M. Laniado, W. Schörner, C. Claussen, H.J. Weinmann: Gadolinium-DTPA: A new contrast agent for magnetic resonance imaging, Radiat. Med. **3**(1), 7–12 (1985)
23.33 D.G. Gadian, J.A. Payne, D.J. Bryant, I.R. Young, D.H. Carr, G.M. Bydder: Gadolinium-DTPA as a contrast agent in MR imaging–theoretical projections and practical observations, J. Comput. Assist. Tomogr. **9**(2), 242–251 (1985)
23.34 J. Hennig, A. Nauerth, H. Friedburg, D. Ratzel: Ein neues Schnellbildverfahren für die Kernspintomographie, Radiologe **24**, 579–580 (1984)
23.35 P.S. Melki, R.V. Mulkern, L.P. Panych, F.A. Jolesz: Comparing the FAISE method with conventional dual-echo sequences, J. Magn. Reson. Imaging **1**, 319–326 (1991)
23.36 R.T. Constable, J.C. Gore: The loss of small objects in variable TE imaging: Implications for FSE,RARE, and EPI, Magn. Reson. Med. **28**, 9–24 (1992)
23.37 A. Haase, J. Frahm, D. Mathaei, et al.: FLASH imaging. Rapid imaging using low flip-angle pulses, J. Magn. Reson. **67**, 256–266 (1986)
23.38 E.M. Haacke, Y. Xu, Y.C. Cheng, J.R. Reichenbach: Susceptibility weighted imaging (SWI), Magn. Reson. Med. **52**(3), 612–618 (2004)
23.39 S. Ogawa, T.M. Lee, A.R. Kay, D.W. Tank: Brain magnetic resonance imaging with contrast dependent on blood oxygenation, Proc. Natl. Acad. Sci. USA **87**(24), 9868–9872 (1990)
23.40 S. Ogawa, R.S. Menon, D.W. Tank, S.G. Kim, H. Merkle, J.M. Ellermann, K. Ugurbil: Functional brain mapping by blood oxygenation level-dependent contrast magnetic resonance imaging. A comparison of signal characteristics with a biophysical model, Biophys. J. **64**(3), 803–812 (1993)
23.41 R.C. Brasch: Work in progress: methods of contrast enhancement for NMR imaging and potential applications. A subject review, Radiology **147**(3), 781–788 (1983)
23.42 L. Knutsson, F. Ståhlberg, R. Wirestam: Absolute quantification of perfusion using dynamic susceptibility contrast MRI: pitfalls and possibilities, MAGMA **23**(1), 1–21 (2010)
23.43 D.D. Stark, J. Wittenberg, M.S. Middleton, J.T. Ferrucci Jr.: Liver metastases: Detection by phase-contrast MR imaging, Radiology **158**(2), 327–332 (1986)
23.44 W.R. Nitz: Fast and ultrafast non-echo-planar MR imaging techniques, Eur. Radiol. **12**(12), 2866–2882 (2002)
23.45 G.M. Bydder, J.M. Pennock, R.E. Steiner, S. Khenia, J.A. Payne, I.R. Young: The short TI inversion recovery sequence – An approach to MR imaging of the abdomen, Magn. Reson. Imaging **3**(3), 251–254 (1985)
23.46 B. De Coene, J.V. Hajnal, P. Gatehouse, D.B. Longmore, S.J. White, A. Oatridge, J.M. Pennock, I.R. Young, G.M. Bydder: MR of the brain using fluid-attenuated inversion recovery (FLAIR) pulse sequences, Am. J. Neuroradiol. **13**(6), 1555–1564 (1992)
23.47 E.O. Stejskal, J.E. Tanner: Spin diffusion measurements: Spin echoes in the presence of a time-dependent field gradient, J. Chem. Phys. **42**(1), 288–292 (1965)
23.48 P.J. Basser, J. Mattiello, D. LeBihan: MR diffusion tensor spectroscopy and imaging, Biophys. J. **66**(1), 259–267 (1994)
23.49 S. Mori, B.J. Crain, V.P. Chacko, P.C. van Zijl: Three-dimensional tracking of axonal projections in the

brain by magnetic resonance imaging, Ann. Neurol. **45**(2), 265–269 (1999)
23.50 F.G. Shellock: Magnetic Resonance Procedures: Health Effects and Safety (2001), 450pp.
23.51 H.J. Wagner, M. Kalinowski, K.J. Klose, H. Alfke: The use of gadolinium chelates for x-ray digital subtraction angiography, Invest. Radiol. **36**(5), 257–265 (2001), ,
23.52 H.J. Wagner, M. Kalinowski, K.J. Klose, H. Alfke: Erratum for H.J. Wagner et al., Invest. Radiol. **36**(5), 257–265, Invest. Radiol. **36**(9), 553 (2001)
23.53 T. Grobner: Gadolinium – A specific trigger for the development of nephrogenic fibrosing dermopathy and nephrogenic systemic fibrosis, Nephrol. Dial. Transplant. **21**, 1104–1108 (2006)
23.54 T. Grobner: Erratum for Grobner, Nephrol. Dial. Transplant. **21**(4), 1104–1108, Nephrol. Dial. Transplant. **21**(6), 1745 (2006)